SEPARATED FLOW PHYSICS USING FREQUENCY ANALYSIS AND MODAL DECOMPOSITION

Anushka Subedi
SEMTE
Arizona State University
asubedi5@asu.edu

Tulio R. Ricciardi
SEMTE
Arizona State University
tulio.ricciardi@asu.edu

Yulia T. Peet
School for Engineering of Matter, Transport, and Energy
Arizona State University
ypeet@asu.edu

ABSTRACT

This paper presents a computational study identifying dominant flow structures, their frequencies, and the correlations with the wall pressure signal in a turbulent backward-facing step. A long-term goal of this study is to identify potential strategies for a design of metamaterials to control flow separation in turbulent flows. We perform Direct Numerical Simulations (DNS) of flow over a backward-facing step at Re_h = 5100 with a spectral-element method. To provide a turbulent inflow to the step, we perform simultaneous auxiliary simulations of a turbulent half-channel flow that intersects with the step domain. We apply spectral analysis to extract dominant spatial and temporal patterns from the flow. We focus on key regions: upstream, near-wake, far-wake, and the recirculation bubble to understand how different flow features, such as shear layer flapping and vortex shedding, are reflected in wall signals. Two main questions guide our work: 1) What are the dominant frequencies driving the separated flow? 2) Where should metamaterial strips be placed to interact with these dynamics? Our results show distinct frequency peaks, with a low-frequency component at $St \approx 0.03$, associated with large-scale recirculation bubble oscillations, and higher-frequency content around $St \approx 0.2$, corresponding to shear-layer flapping dynamics. To further characterize these dynamics, we apply Proper Orthogonal Decomposition (POD) to the pressure field, where the leading modes capture dominant low-frequency behavior consistent with the bubble oscillations observed in the spectra, reinforcing the link between pressure signals and coherent flow structures. These findings suggest that the upstream region and the area beneath the recirculation bubble are promising locations for control, as they exhibit strong, coherent signatures in the pressure field. The identified low- and intermediate-frequency bands ($St \approx 0.03$ and $St \approx 0.2$) provide relevant targets for the design of metamaterial-based flow control strategies.

INTRODUCTION

Flow separation and reattachment over a backward-facing step (BFS) create complex turbulent features such as shear layers, recirculation patterns, and vortex shedding (Le *et al.* (1997)). These structures strongly influence wall pressure and shear stress signals, offering cues about the unsteady behavior of the flow. Although BFS has been widely studied, relating the unsteady features to the surface responses that may guide design of passive surfaces and metamaterials for separation control remains an active area of research.

Separation typically occurs when an adverse pressure gradient or sudden geometric expansion causes the boundary layer to detach from the surface (Williams (1977)). This results in increased drag, loss of lift, and strong unsteady fluctuations in velocity and pressure throughout the separated region (Simpson (1981); Theofilis & Colonius (2004)). These fluctuations can cause additional problems, including flow-induced vibrations and resonance in cavities, noise amplification (Cattafesta *et al.* (2008)), and aero-optical distortions (Kalensky *et al.* (2024)). To suppress separation and its consequences, several control methods have been developed. Active methods like blowing, suction, synthetic jets, and fluidic oscillators have proven effective (Schatz *et al.* (2004); Glezer & Amitay (2002); Raghu (2013)), but they require external energy, sensors, actuators, and complex control hardware (Gad-el Hak & Bushnell (1991)). Passive methods, such as compliant surfaces (Gad-el Hak (2002)), eliminate energy requirements but are often limited by large deformations and unpredictable dynamic behavior.

This study is motivated by the promising prospect of developing a new passive strategy based on resonant metamaterials for flow separation control. Metamaterials are engineered materials that can be tuned to block or enhance flow perturbations at specific frequencies without requiring large structural deformations (Hussein *et al.* (2015)). Their frequency-selective response makes them a promising candidate for controlling turbulent and separated flows in a fully passive manner. Our long-term goal is to use resonant metamaterials to reduce flow separation and a related unsteadiness in BFS configurations. As a first step, this study uses Direct Numerical Simulations (DNS) to identify the dominant flow structures, their frequencies, and their spatial footprints. These insights will help determine the optimal locations and target frequencies for placing metamaterial strips, enabling effective and efficient passive flow control.

NUMERICAL METHODS

We use the code Nek5000 (Fischer *et al.* (2015)) to perform Direct Numerical Simulations, which is a highly scalable, open-source spectral-element CFD solver. We solve the incompressible Navier–Stokes equations:

$$\frac{\partial \mathbf{u}}{\partial t} + \mathbf{u} \cdot \nabla \mathbf{u} = -\nabla p + \nu \nabla^2 \mathbf{u}, \quad \nabla \cdot \mathbf{u} = 0, \qquad (1)$$

where, $\mathbf{u}$ is the velocity field, p is the pressure, and ν is the kinematic viscosity. Time integration uses a third-order backward differentiation scheme for viscous terms and extrapolation for nonlinear terms. The pressure is computed via a pressure-Poisson formulation with a projection method (Fischer, 1997).

The computational domain consists of a turbulent half-channel with periodic boundaries overlapping with the BFS domain. The turbulent velocity profile from the half-channel is supplied as the time-dependent inflow condition for the turbulent BFS. The bottom wall in the BFS domain, including the step, is treated as no-slip, the top wall as a symmetry plane, the outlet is traction-free, and periodic boundary conditions are applied in the spanwise direction. The flow has a Reynolds number of $Re_h = 5100$. The half-channel domain has dimensions $2\pi H \times H \times \pi H$ (H is the channel half height), while the BFS domain is split into an upstream part with the dimensions $10h \times 2.5h \times 7.85h$ ($h = 0.4H$ is the step height), and the downstream part with the dimensions $20h \times 3.5h \times 7.85h$. The coordinates of the step corner are set to $(x, y) = (0, h)$. We use high-order polynomial expansions of 7th order in each element for the half-channel and BFS domains.

RESULTS

We first validate the numerical setup through a grid convergence study using three meshes comprising 5 million, 21 million, and 52 million grid points (Grids 1-3). The results are presented in Figures 1 – 4, where a comparison with the DNS data of Le *et al.* (1997) at the same Reynolds number of $Re_h = 5100$ is also included. We note, however, that the DNS of Le *et al.* (1997) is performed under different inflow conditions of incoming turbulent boundary layer as opposed to a half-channel inflow in the current study. Their data are thus included for reference purposes only, and collapse of the profiles is not expected. Grid 2 demonstrates good convergence in mean velocity and Reynolds stress profiles and is therefore used for all subsequent analysis.

The overall structure of this flow can be visualized in Figures 5 and 9 - 11. A dominant feature is the recirculation bubble shown in Figure 5, whose length of $6.25h$ in the present study is similar to the bubble length of $6.28h$ in Le *et al.* (1997). Figure 9 shows the mean streamwise velocity, while Figures 10 and 11 present the instantaneous streamwise velocity and pressure in this flow. All these figures capture the dominant BFS structures: the fluctuating shear-layer developing from the step corner and the low-speed recirculation region underneath.

To investigate the unsteady characteristics of the flow, pressure signals were recorded at multiple probe locations

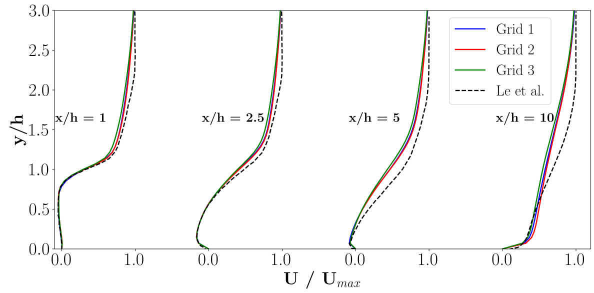

Figure 1. Profiles of mean streamwise velocity as compared to Le *et al.* (1997).

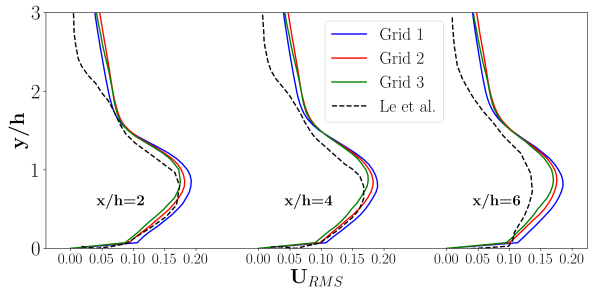

Figure 2. Profiles of U_{RMS} as compared to Le *et al.* (1997).

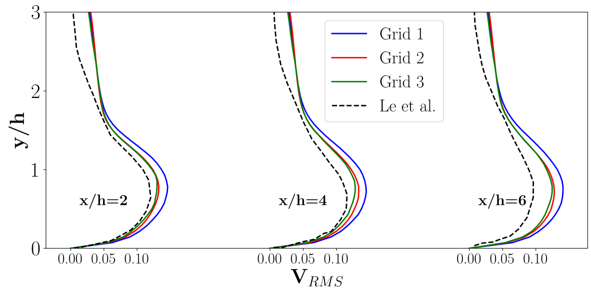

Figure 3. Profiles of V_{RMS} as compared to Le *et al.* (1997).

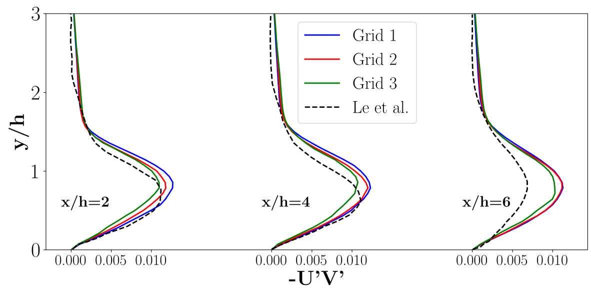

Figure 4. Profiles of u'v' as compared to Le *et al.* (1997).

along the bottom wall and within the flow, as shown in Figure 9. These probes are placed to capture turbulent fluctuations across the upstream, separation bubble, near wake, and far wake regions. We define a non-dimensional time based on a convective time scale related to the step height as $t^* = tU_c/h$, where h is the step-height and U_c is the centerline velocity. The initial 250 non-dimensional time units are discarded to eliminate transient effects, and the subsequent 1750 non-dimensional time units are used for the spectral analysis. The pressure signals are sampled at a rate of 15 samples per 1 t^* to

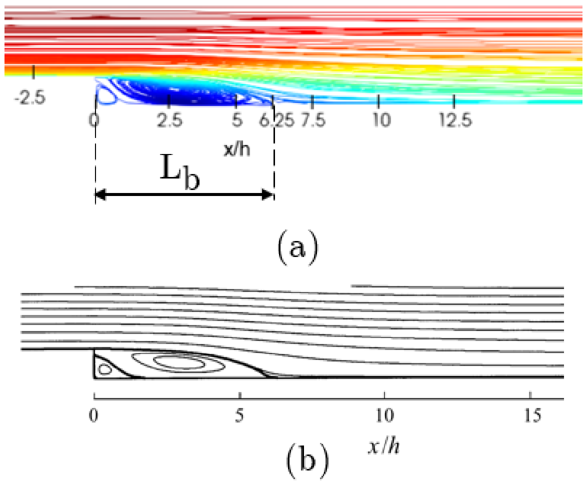

Figure 5. Comparison of mean flow velocity streamlines with DNS of Le *et al.* (1997). Bubble size: (a) $L_b = 6.25h$ in the current DNS; (b) $L_b = 6.28h$ in Le *et al.* (1997).

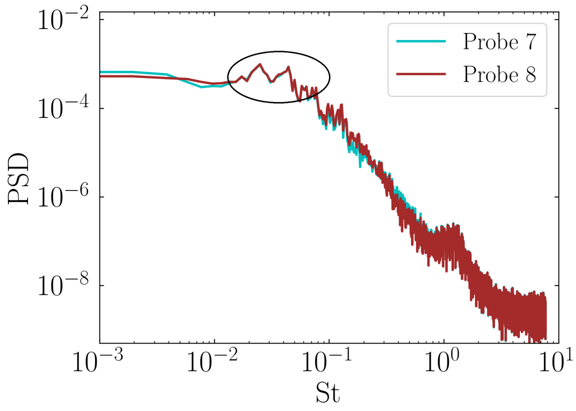

Figure 6. Power spectral density (PSD) of pressure for bubble probes 7 and 8.

ensure an adequate temporal resolution.

A sample pressure signal at two wall probes and its resulting spectra are shown in Figure 12, while Figures 6 and 7 document the PSD of the pressure signal at selected bubble and wake probes, respectively. The resulting spectra show a dominant low-frequency behavior across all probe locations. No distinct higher-frequency peaks are observed in the raw pressure spectra. Instead, a coherent low-frequency band in the range St $\approx$ 0.03–0.05 is present across multiple regions, including the near-wake (Probes 1, 2 and 3), far-wake (Probes 5 and 6), within the recirculation bubble (Probes 7 and 8), and upstream of the step (Probe 9). This consistent signature suggests that the flow dynamics are dominated by large-scale, low-frequency oscillations associated with recirculation bubble breathing.

The absence of clear higher-frequency peaks, typically attributed to shear-layer flapping or vortex shedding, may indicate that such dynamics are either weaker, more broadband in nature, or not strongly reflected in the wall-pressure signal in the current flow configuration. Additionally, the dominance of low-frequency content suggests that the pressure field is primarily influenced by global flow motions rather than localized shear-layer instabilities.

To extract the dominant coherent structures, a two-dimensional Proper Orthogonal Decomposition (POD) (Taira *et al.*, 2017) is performed on pressure snapshots collected across the central plane in a spanwise direction over a selected subdomain, consisting of the region upstream of the step, $(x,y) = [-3.75h, 0] \times [h, 1.5h]$, and downstream of the step and the recirculation bubble, $(x,y) = [0, 12.5h] \times [0, 1.5h]$ as indicated in Figure 9. This reduced domain focuses on the dynamically relevant regions while limiting computational cost. The analysis is conducted using the same statistically stationary dataset described for the spectral analysis, where the initial 250 non-dimensional time units are discarded and the subsequent 1750 non-dimensional time units are retained. Snapshots for POD are taken at one sample per 0.64 t^*.

The leading POD modes and their spatial structure are shown in Figure 13, with the corresponding power spectral density (PSD) of their temporal coefficients. The energy distribution shown in Figure 8 indicates that the first mode captures approximately 8.5% of the total energy, while the second and third modes each contribute about 7.5%, suggesting a relatively distributed energy content across modes rather than a single dominant structure. The spatial structure of the first mode is relatively broad and diffuse, indicating large-scale coherent motion associated with the low-frequency dynamics of the separation bubble. The second and third modes exhibit similar large-scale structures with a spatial phase shift relative to one another, which is characteristic of oscillatory dynamics and shows a paired mode behavior associated with the breathing motion of the recirculation zone. Higher-order modes (e.g., modes 5 and 10) are more localized within the separated shear layer and do not extend to the wall, indicating their stronger association with shear-layer instabilities.

Power spectral density analysis of the temporal coefficients reveals that the dominant contribution across the leading modes corresponds to a low-frequency content in the range St $\approx$ 0.03–0.05, consistent with the spectra obtained from the pressure signals and indicative of the recirculation bubble breathing dynamics. The shear flapping frequencies appear in higher-order POD modes as secondary peaks in the range St $\approx$ 0.2–0.6. This suggests that, although the spatial modes resemble shear-layer-type structures, their temporal evolution is largely governed by the global recirculation bubble oscillations. This indicates that the dominant dynamics captured by POD are associated with large-scale, low-frequency motions rather than distinct shear-layer instabilities. However, it is also important to note that POD alone does not provide a clear separation of dynamics at specific frequencies. A more precise characterization of frequency-dependent coherent structures would require spectral POD (SPOD), which can directly link spatial modes to distinct frequency bands, planned for the future work.

Since these dominant low-frequency dynamics are most strongly reflected in the upstream region and beneath the recirculation bubble, these locations emerge as key targets for flow control. Hence, the suggested control frequencies and locations could be as listed in Table 1.

Table 1. Dominant frequencies and locations

Probe	Location	Strouhal Modes
9	Upstream wall	0.03-0.05, 0.2-0.6
6	Under the bubble	0.03-0.05, 0.2-0.6

CONCLUSION

Direct Numerical Simulations of turbulent flow over a backward-facing step at $Re_h = 5100$ were performed to investigate the dominant flow dynamics and their signatures in wall-pressure signals, with the objective of informing flow control strategies. A combination of spectral analysis and Proper Orthogonal Decomposition (POD) was used to characterize the unsteady behavior of the flow. The spectral analysis consistently identifies low-frequency content in the range St $\approx$ 0.03–0.05, associated with recirculation bubble oscillations as the primary energetic contribution. These dynamics are most strongly reflected in the upstream region and beneath the recirculation bubble, suggesting these locations as promising targets for control strategies.

The POD results further support this observation by capturing dominant large-scale coherent structures associated with these low-frequency motions, while also indicating the presence of weaker higher-frequency components in the range St $\approx$ 0.2–0.6, which may be attributed to shear-layer flapping. However, the relatively low energy content of individual POD modes and the absence of strongly dominant higher-frequency peaks in the spectra suggest that the flow is primarily governed by global, low-frequency dynamics rather than localized, high-frequency instabilities in this configuration. These additional higher-frequency components could still be considered in the design of control mechanisms, although their influence appears secondary compared to the dominant low-frequency behavior.

The agreement between spectral and modal analyses shows the central role of recirculation bubble dynamics in governing the unsteady separated flow and their clear imprint on wall-pressure signals. These findings provide a basis for targeting specific frequency bands and spatial regions in the design of metamaterial-based surface modifications for controlling flow separation. Future work will focus on applying frequency-resolved techniques such as SPOD to more clearly isolate coherent structures at specific frequencies.

ACKNOWLEDGEMENT

This work is supported by the US AFOSR (AFOSR FA9550-23-1-0762) with program manager Dr. Gregg Abate. Computational resources are provided by Texas Advanced Computing Center's Stampede3, and Arizona State University's Sol supercomputers.

REFERENCES

Cattafesta, Louis N., Song, Qi, Williams, David R., Rowley, Clarence Worth & Alvi, Farrukh S. 2008 Active control of flow-induced cavity oscillations. *Progress in Aerospace Sciences* **44** (7-8), 479–502.

Fischer, P., Lottes, J., Kerkemeier, S., Marin, O., Heisey, K., Obabko, A., Merzari, E. & Peet, Y. 2015 Nek5000: User's manual. *ANL Report No. ANL/MCS-TM-351* .

Fischer, P. F. 1997 An overlapping Schwarz method for spectral element solution of the incompressible Navier–Stokes equations. *J. Comp. Physics* **133** (1), 84–101.

Glezer, A. & Amitay, M. 2002 Synthetic jets. *Annual Review of Fluid Mechanics* **34**, 503–529.

Gad-el Hak, M. 2002 Compliant coatings for drag reduction. *Progress in Aerospace Sciences* **38**, 77–99.

Gad-el Hak, M. & Bushnell, D. M. 1991 Separation control: Review. *Journal of Fluids Engineering* **113** (1), 5–30.

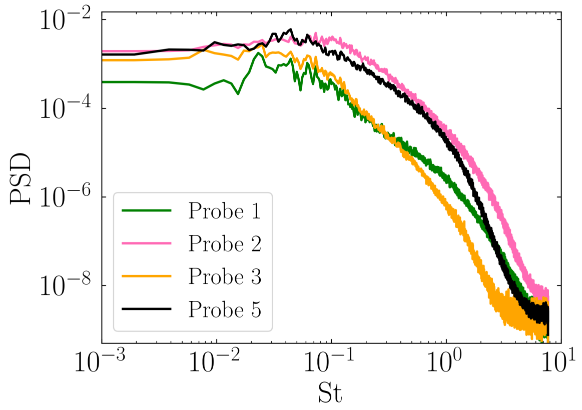

Figure 7. Power spectral density (PSD) of pressure for wake probes 1, 2, 3, and 5.

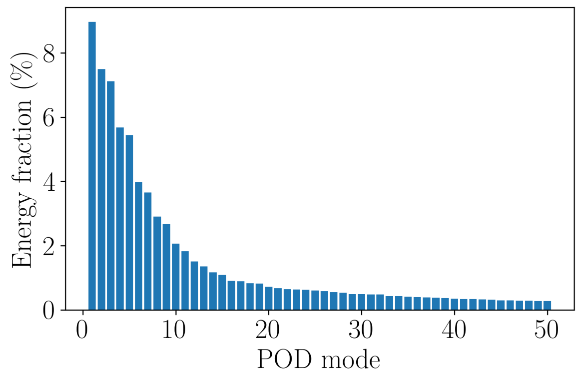

Figure 8. Energy content of leading POD modes

Hussein, M. I., Biringen, S., Bilal, O. R. & Kucala, A. 2015 Flow stabilization by subsurface phonons. *Proceedings of the Royal Society A* **471** (2177), 20140928.

Kalensky, Matthew, Gordeyev, Stanislav, Kemnetz, Matthew R. & Spencer, Mark F. 2024 Aero-optical effects, part ii. sources of aberrations: tutorial. *J. Opt. Soc. Am. A* **41** (11), 2175–2187.

Le, H., Moin, P. & Kim, J. 1997 Direct numerical simulation of turbulent flow over a backward-facing step. *Journal of Fluid Mechanics* **330**, 349–374.

Raghu, S. 2013 Fluidic oscillators for flow control. *Experiments in Fluids* **54**, 1455.

Schatz, M., Thiele, F., Petz, R. & Nitsche, W. 2004 Separation control by periodic excitation and its application to a high-lift configuration. In *2nd AIAA Flow Control Conf.*, p. 2507.

Simpson, R. L. 1981 Review—a review of some phenomena in turbulent flow separation. *J. Fluids Eng.* **103** (4), 520–533.

Taira, K., Brunton, S. L., Dawson, S. T. M., Rowley, C. W., Colonius, T., McKeon, B. J., Schmidt, O. T., Gordeyev, S., Theofilis, V. & Ukeiley, L. S. 2017 Modal analysis of fluid flows: An overview. *AIAA Journal* **55** (12), 4013–4041.

Theofilis, Vassilis & Colonius, Tim 2004 Three-dimensional instabilities of compressible flow over open cavities: Direct solution of the biglobal eivenvalue problem. In *34th AIAA Fluid Dynamics Conference and Exhibit*, p. 2544.

Williams, III, J. C. 1977 Incompressible Boundary-Layer Separation. *Annual Review of Fluid Mechanics* **9**, 113–144.

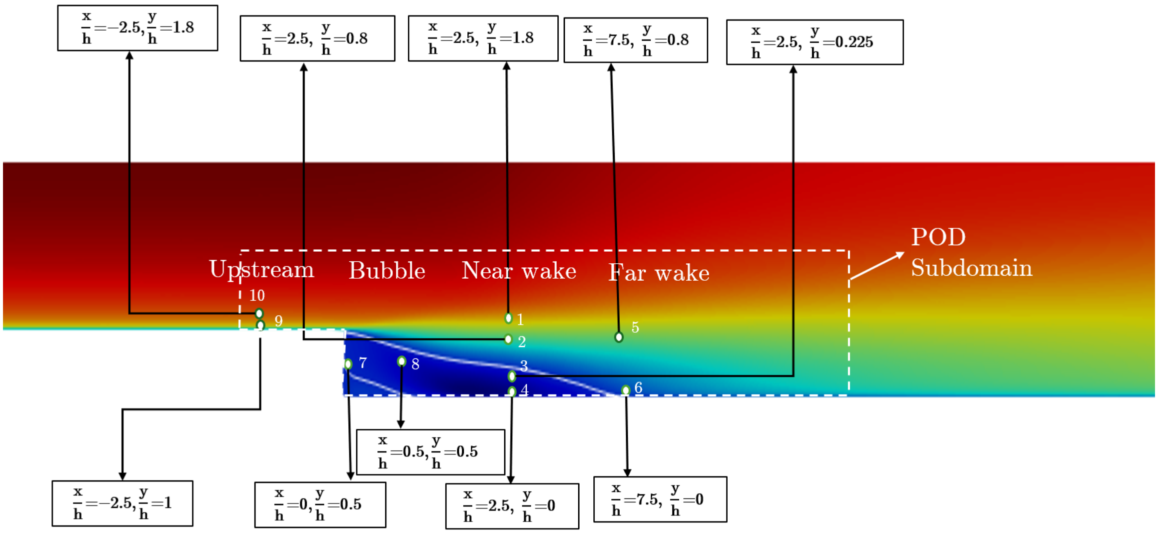

Figure 9. Probe locations within four different regions. Near wake region: probes 1, 2, 3, and 4; Far wake region: probes 5 and 6; Bubble region: probes 7 and 8; Upstream of the step: probes 9 and 10. White dashed lines denotes the region used for POD analysis.

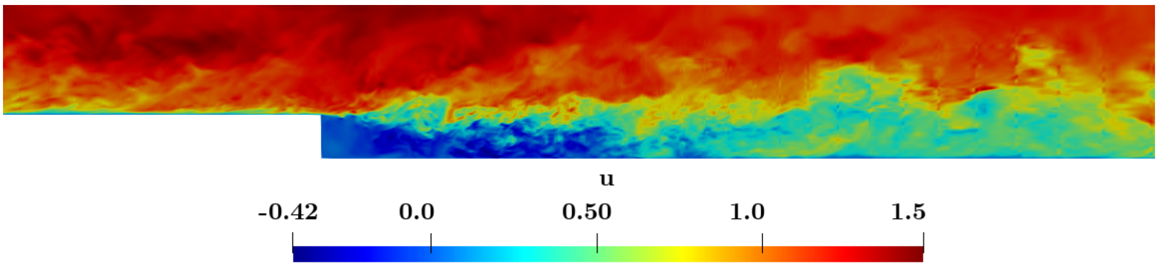

Figure 10. Contours of instantaneous streamwise velocity field

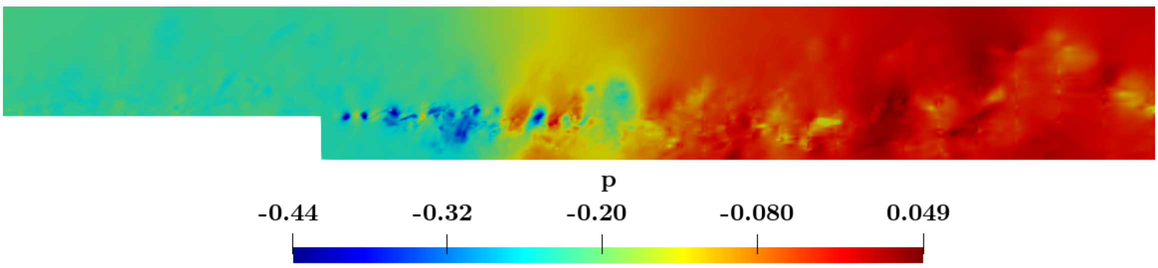

Figure 11. Contours of instantaneous pressure field

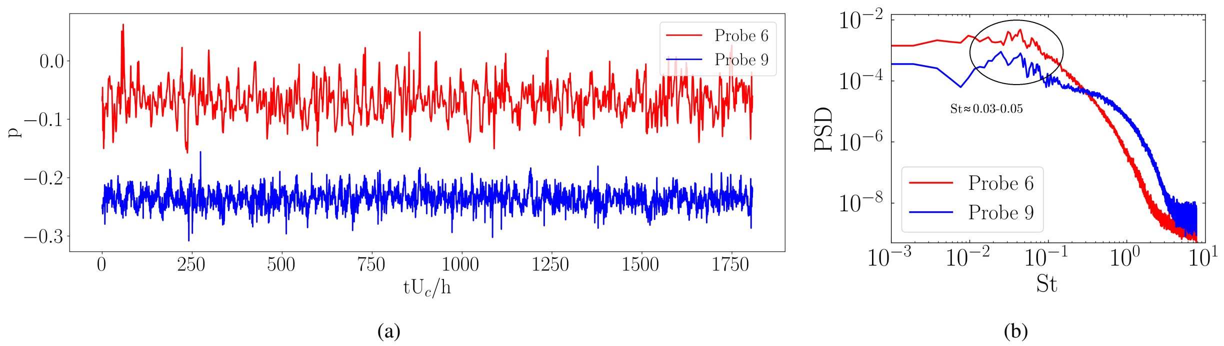

Figure 12. (a) Pressure time series at wall probes 6 (red) and 9 (blue), shown in non-dimensional time units $t^* = tU_c/h$. (b) Corresponding power spectral density (PSD). The two probes are identified as optimal sensing locations for flow control.

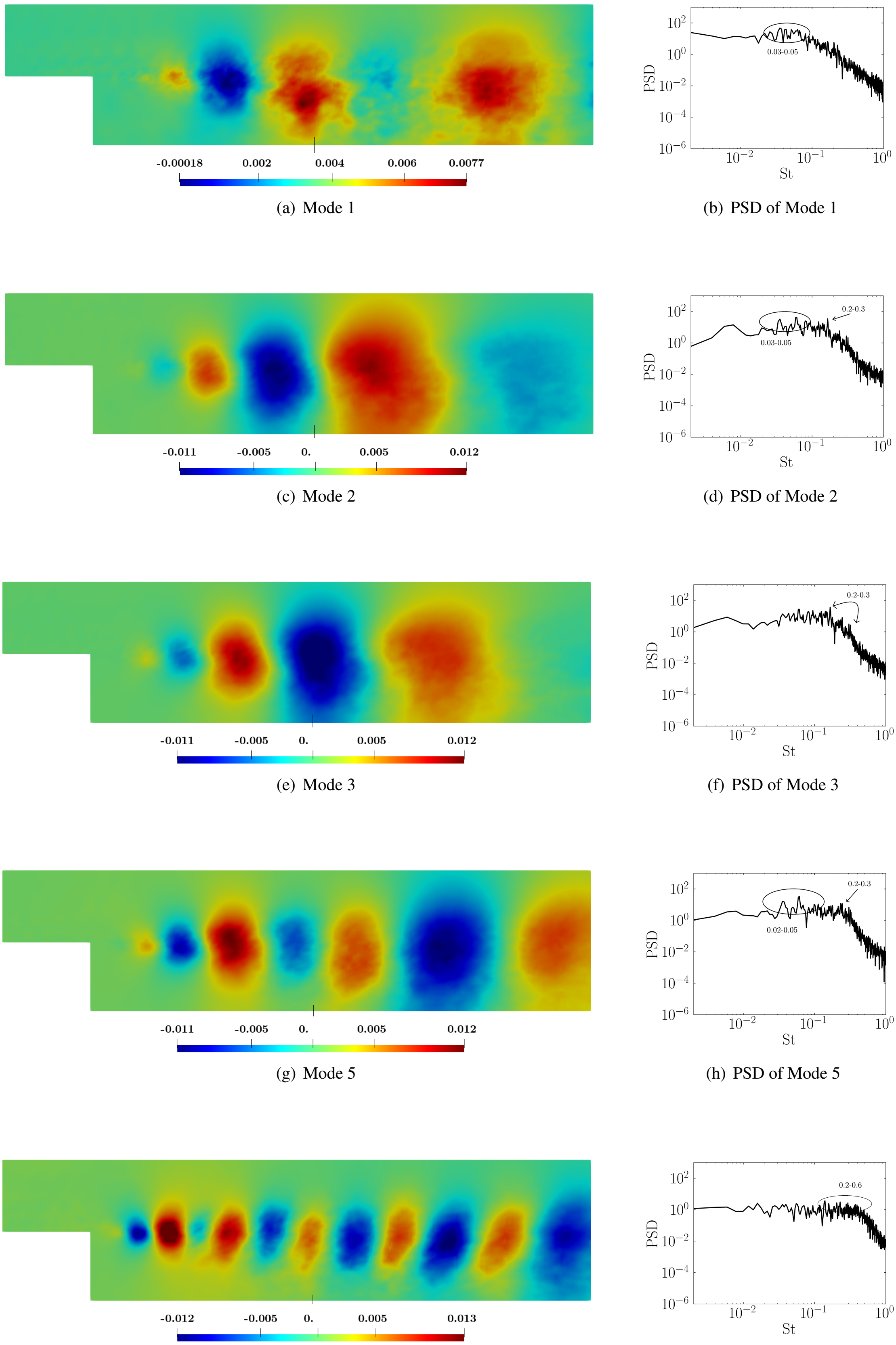

(a) Mode 1 (b) PSD of Mode 1

(c) Mode 2 (d) PSD of Mode 2

(e) Mode 3 (f) PSD of Mode 3

(g) Mode 5 (h) PSD of Mode 5

(i) Mode 10 (j) PSD of Mode 10

Figure 13. Left: POD modes of pressure with (a) mode 1, (c) mode 2, (e) mode 3, (g) mode 5 and (i) mode 10. Black vertical ticks on the wall denote the edge of the separation bubble. Right: PSD of the temporal coefficients of the respective modes on the left i.e. (b) PSD of mode 1, (d) PSD of mode 2, (f) PSD of mode 3 (g) PSD of mode 5 and (j) PSD of mode 10.